DEVELOPMENT OF COMPUTATIONAL FLUID-STRUCTURE INTERACTION METHOD FOR YACHT SAILS

F.M.J. Bergsma, N. Moerke and **K.S. Zaaijer**, Van Oossanen Naval Architects, Netherlands, f.bergsma@oossanen.nl, n.moerke@oossanen.nl, s.zaaijer@oossanen.nl
H.W.M. Hoeijmakers, University of Twente, Netherlands, h.w.m.hoeijmakers@utwente.nl

SUMMARY

This paper presents a Fluid-Structure Interaction (FSI) method for sails. In this FSI method the pressure field around the sail is determined using the Computational Fluid Dynamics (CFD) package FINE/Marine using the ISIS solver. This computational method is based on the Reynolds-Averaged Navier-Stokes Equations (RANSE). The computed pressure field serves as input for a basic structural model implemented in the Nastran-based Finite Element Analyses (FEA) package Femap which determines the deformation of the sail subject to the aerodynamic load. In an iterative procedure the distribution of the surface pressure and the deformation of the sail attain a stable equilibrium. The aim of the FSI method is to determine the steady flying shape of the sail and to obtain the aerodynamic forces generated by the sail taking into account the deformation of the sail.

A method is presented for 2D sail sections as well as a method for 3D upwind sails. These methods are capable of determining the steady deformation of the sail. The results of the method for 2D sail sections are compared with a set of experimental data. This comparison shows that the deformed shape of a 2D mast and sail section compares satisfactorily with measured data for various combinations of slackness and angles of attack.

NOMENCLATURE

$\vec{c}$	sample point
c	chord length (m)
E	elasticity modulus (N·m^{-2})
$\vec{g}$	gravitational acceleration (m·s^{-2})
K	turbulence kinetic energy (m^2·s^{-2})
l	cloth length (m)
$\vec{n}$	outward bound normal vector (-)
n_s	number of sample points in RBF (-)
p	pressure field (N·m^{-2})
Re	Reynolds number (-)
S	control volume surface (m^2)
$\bar{\bar{S}}$	rate of strain tensor (s^{-1})
s	slackness (-)
$\vec{U}$	velocity field (m·s^{-1})
$\vec{U}_d$	velocity of surface S (m·s^{-1})
$\overrightarrow{u'}$	flow velocity fluctuation (m·s^{-1})
$u(\vec{x})$	deformation (m)
V	air speed (m·s^{-1})
V	control volume (m^3)
w_i	weighting factor in RBF (-)
$\vec{x}$	interpolated point (m)
y^+	dimensionless distance from wall (-)
α	angle of attack (°)
ε	excess cloth length (m)
μ	air dynamic viscosity (Pa·s)
μ_t	turbulent viscosity (Pa·s)
ν	Poisson ratio (-)
ρ	density (kg·m^{-3})
$\bar{\bar{\tau}}$	stress tensor (N·m^{-2})
$\bar{\bar{\tau}}_l$	viscous stress tensor (N·m^{-2})
$\bar{\bar{\tau}}_t$	Reynolds stress tensor (N·m^{-2})
ϕ	radial basis function (m)

1 INTRODUCTION

Currently most procedures for sail design, i.e. providing planform, camber and cloth selection, are based on experience. Mostly crude analytical models and models based on a regression of previous wind tunnel tests are used to predict the lift and drag forces on sails. In the analysis of the aerodynamic performance of sail designs only a few designers use computational methods. These are usually based on potential flow methods for predetermined shapes. Since the deformation of the sail due to aerodynamic loads can be substantial, improvements in the prediction of the aerodynamic performance of sails can be achieved by using Fluid-Structure Interaction (FSI) analysis. FSI is the interaction between a deformable structure and the flow surrounding it. FSI is regarded as a frontier in numerical methods for sailing [1].

The flying shape is determined by the structural properties of the sail and the pressure distribution on the sail produced by the flow around the sail. A common approach is the so-called ‘segregated’ or ‘partitioned’ approach. This means that first the flow around a given shape of the sail and corresponding flow domain is solved using Computational Fluid Dynamics (CFD). This yields the pressure distribution on the sail. This pressure distribution is exported to a structural method (Finite Element Method), which solves for the deformed shape under the specified load.

The deformed shape is used to update the flow domain and the flow around the new geometry is calculated. This process repeats in an iterative manner until convergence of the sail shape and the flow is attained.

The first efforts in fluid structure interaction were made by Schoop [2] [3] [4] and Fukasawa and Katori [5]. Vortex Lattice potential flow models were coupled with linear elastic models for the sails. The applicability of the used models can be questioned, but more computational power was required to introduce viscous flow models and non-linear elastic models for the structural behaviour of the sail [6].

From 2008 on, a new generation of FSI methods was introduced. These models are based on viscous flow CFD solvers, combined with more advanced models for the structural behaviour of the sail. In 2008 Renzsch, Muller and Graf presented a fluid structure interaction method for downwind sails [7]. A RANSE solver was combined with the self-developed code FlexSail for the structural behaviour of the sails. A wrinkling model was introduced to cope with compressional loads in the sails [8]. Paton Morvan and Heppel described the coupling between the RANS method CFX and a purpose-built code called RELAX for membrane structures aimed to model the structural behaviour of sails [9]. In 2011 the same structural model was weakly coupled to the RANSE solvers FLUENT and OpenFOAM [10].

Trimarchi et al. developed a weak coupling between the unsteady RANS solver OpenFOAM and a structural method that uses shell elements instead of the more common membrane elements. These shell elements are able to capture the wrinkling of the sail better [11].

A new approach to the coupling of the structural and the fluid model was applied recently by Lombardi, et al.. Instead of the commonly used weak coupling, the FSI problem is solved using a strongly coupled segregated approach. This is achieved by introducing a sub-iteration cycle for every iteration step. This is necessary to prevent numerical instability which occurs for large deformations [12].

Meanwhile, a strong coupling was established between the inviscid flow solver AVANTI with the structural model ARA which uses membrane elements. Validation was performed by comparing numerical results with the data from full scale tests. Comparison of the sail shape for the steady case showed good correspondence. [13]

The aim of the work presented here is to develop and validate a method to predict the flying shape of the sail under steady conditions. Results of both 2D and 3D cases are presented. Numerical simulation for 3D FSI has been performed to investigate the capabilities of the FSI method, but crude methods are used for the prediction of the deformation. Three main topics are covered: the CFD method that is used to predict the pressure field around a sail; the structural method used to predict the deformation of a sail; and the computational procedure that handles the iterative process and the transfer of data between the structural method and the CFD method.

2 CFD METHOD

In this section a description is given of the CFD method used to determine the flow. First the governing equations are given. This is followed by a description of the computational domain and the boundary conditions, and of the mesh. The geometry and flow conditions for the 2D and 3D case are given.

2.1 GOVERNING EQUATIONS

The modelling of the viscous-flow is based on Reynolds Averaged Navier Stokes equations (RANSE) for the incompressible-unsteady turbulent flow. This is done using the ISIS solver from the FINE/Marine package [14]. The equation for mass conservation is given in integral conservation form by:

$$\frac{\partial}{\partial t}\int_V \rho dV + \int_S \rho\left(\vec{U} - \vec{U}_d\right)\cdot\vec{n}dS = 0$$

The equation of conservation of momentum is given by:

$$\frac{\partial}{\partial t}\int_V \rho\vec{U}dV + \int_S \rho\vec{U}\left[\left(\vec{U} - \vec{U}_d\right)\cdot\vec{n}\right]dS = \int_S \left(\bar{\bar{\tau}} - p\cdot\bar{\bar{I}}\right)\cdot\vec{n}dS + \int_V \rho\vec{g}dV$$

Closure of this set of equations is obtained by defining the stress tensor:

$$\bar{\bar{\tau}} = \bar{\bar{\tau}}_t + \bar{\bar{\tau}}_l$$

Here $\bar{\bar{\tau}}_t$ is the Reynolds stress tensor and $\bar{\bar{\tau}}_l$ the viscous stress tensor. The viscous stress tensor is defined as:

$$\bar{\bar{\tau}}_l = 2\mu\left(\bar{\bar{S}} - \frac{1}{3}\bar{\bar{I}}\vec{\nabla}\cdot\vec{U}\right)$$

Here $\bar{\bar{S}}$ is the rate of strain tensor. The Reynolds stress tensor is defined as:

$$\bar{\bar{\tau}}_t = -\rho\overrightarrow{u'}\cdot\overrightarrow{u'}$$

A closure of this term is required to solve the set of equations. Turbulence viscosity models are used for this closure. These models are based on the Boussinesq approximation. This commonly used approximation gives the Reynolds stress as follows:

$$\bar{\bar{\tau}}_t = 2\mu_t\left(\bar{\bar{S}} - \frac{1}{3}\bar{\bar{I}}\,\vec{\nabla}\cdot\vec{U}\right) - \frac{2}{3}\rho K\bar{\bar{I}}$$

The SST-Menter turbulence model is used. This model is most suitable for both upwind and downwind sails [15].

2.2 DOMAIN AND BOUNDARY CONDITIONS

The size of the domains used for 2D and 3D cases is tabulated in Table 1. For the 2D case the size of the domain in spanwise (up-down) direction is set to unity. For the 3D case the bottom of the domain is placed ½ chord length below the foot of the sail. This represents the water surface. The size of the computational domain followed from a study on the effect the size on the computed forces on the sail.

Table 1 – Computational domains in chord lengths c.

	Domain size (c)	
	2D	3D
Upstream	50	8
Downstream	80	14
Transverse	50	8
Up	-	12
Down	-	½

The boundary conditions are applied as tabulated in Table 2. The development of the earth's boundary layer is not incorporated. Instead, a symmetry (slip) boundary condition is applied, mimicking the presence of the water surface without generating a surface boundary layer at the bottom of the domain, which would complicate the numerical simulation.

Table 2 – Boundary conditions of computational domain.

	Boundary Condition type	
	2D	3D
Inlet	Far field velocity	Far field velocity
Outlet	Zero pressure gradient	Zero pressure gradient
Transverse	Far field	Far field
Top	Mirror	Far field
Bottom	Mirror	Mirror
Sail/foil	No Slip	No slip

2.3 MESH

Meshes have been generated using HEXPRESS v2.11: a top-down mesher for unstructured hexahedral meshes. For all cases the mesh near solid surfaces is sufficient to maintain a y^+-value of around 1 in boundary layers.

For the 2D case a mesh study has been performed using the NACA0012 wing section. This section is chosen since it has been used for experiments extensively, making it very suitable for validation purposes. A coarse but characteristic mesh for this geometry is shown in Figure 1.

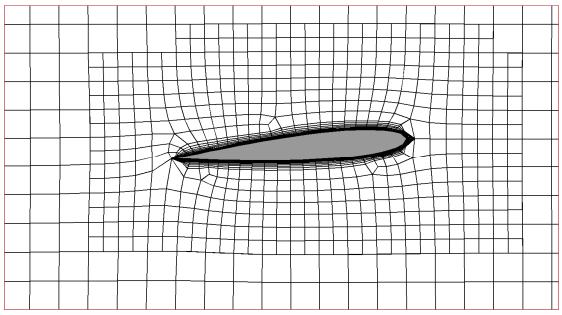

Figure 1 – characteristic mesh for NACA0012 profile, generated with HEXPRESS v2.11.

The number of elements along the chord was varied by increasing the number of refinements. Lift and drag coefficients were determined for various meshes. The results are shown in Table 3.

Table 3 - Lift and drag coefficients for different number of chord-wise elements. NACA0012, Re = $3\cdot10^6$, α=5°, 19 viscous layers, $y^+\approx 1$.

N_{chord}	N_{cell}	C_l	C_d
32	22096	0.5150	0.0217
64	27610	0.5212	0.0146
128	36872	0.5421	0.0109
256	53064	0.5381	0.0103
512	81701	0.5324	0.0101
1024	135330	0.5352	0.0101

It shows that good convergence behavior occurs for the drag coefficient, which converges asymptotically to a value of 0.0101 for meshes with 256 chord-wise elements and more. The lift coefficient does not appear to converge monotonically. This is believed to be due to the unstructured meshing method, but for meshes finer than 512 elements along the chord, the variation of the lift is acceptably small (within 0.5%). This makes it possible to calculate the lift and drag of the section sufficiently accurate.

Experimentally determined values found in literature [16] for the flow around a NACA0012 profile for Re = $3\cdot10^6$ and α= 5° are C_l = 0.54 and C_d = 0.0075. The lift coefficient shows reasonable correspondence. However the drag coefficient is not as accurate. The difference in drag coefficient has been investigated. It was found that the difference is caused by the fact that the computational result is for fully turbulent flow while for the experiments a laminar flow region exists near the leading edge and along a major part of the pressure side of the foil. The higher viscous drag associated with the turbulent flow regime causes an overprediction of the overall drag of the section.

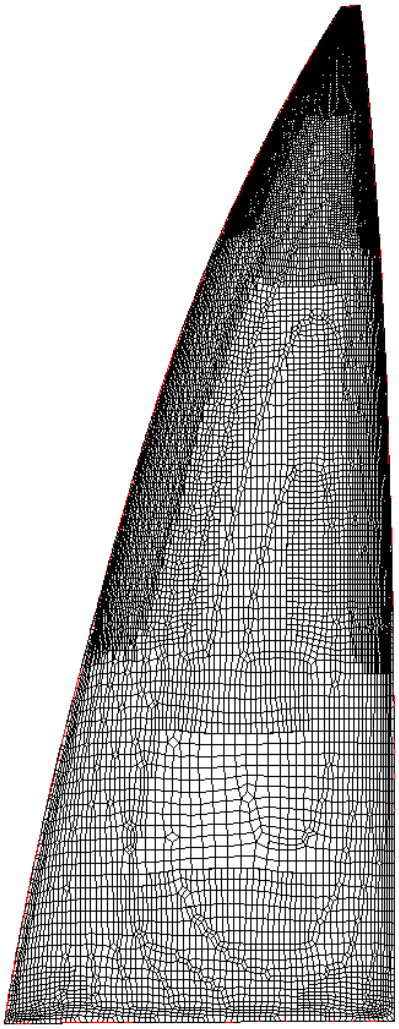

Figure 2 – Typical CFD surface mesh for a sail showing varying refinements along the height and additional refinements at the edges.

For the 3D case a mesh has been generated with a varying number of refinements along the height of the sail. This is necessary because the geometry used has, roughly, a triangular shape. To maintain the specified number of cells along the chord, an increasing number of refinements is required with decreasing chord length of the sail.

In addition, extra refinements along the edge of the sail are applied. Wilkinson [17] showed that these are the regions where flow separation due to high adverse pressure gradients can occur, which can be captured more accurately with the locally refined mesh. It was found that a mesh with 64 elements along the chord and edge refinements gives a good balance between accuracy and computational time. An example of a coarse surface mesh of this type is shown in Figure 2.

A mesh deformation algorithm that is included in the Fine/Marine package is used to adapt the meshes to the deformed sail shape. In FSI the flow needs to be solved for every iteration step taking into account a slightly deformed geometry. Being able to deform the mesh without loss of accuracy omits the need to re-mesh the computational domain every iteration. It was verified that using mesh deformation does not decrease the accuracy of the predicted lift and drag forces of the sail.

2.4 2D GEOMETRY AND FLOW CONDITIONS

The geometry used for 2D numerical simulations is based on the experimental setup by Yam, Karlin & Arieli [18]. The experimental setup is shown in Figure 3.

In the figure the flow direction is from right to left. The chord of the sail is 138 mm and the span 350 mm. The cloth (white) is attached to the leading and trailing edge with two sleeves. At both ends of the wing endplates are mounted parallel to the flow (1) to reduce the 3D behaviour of the flow. The two endplates are connected by two circular rods (2) of 6mm diameter. One of them functions as the leading edge. This is used as pivoting point in order to vary the angle of attack. The trailing edge (3) consists of a 15 mm blade with a thickness of 1.5 mm that is connected to ball bearings that enable the plate to rotate freely around its longitudinal axis.

The sail of the experimental setup consists of a freely rotating trailing edge and a sleeve around the leading edge that is free to rotate around a rod. Accounting for these rotations in the numerical simulations is beyond the scope of the presented research and not relevant for the purpose of simulating the deformation of yacht sails.

In the numerical simulations the leading and trailing edge are therefore considered rigid and fixed. Deformation of the cloth occurs between the two sleeves only. The shape and position of the leading and trailing edge are taken from the experimental data. This is visualized in Figure 4. The blue line shows the geometry as measured for the case of an angle of attack of 4.5° and a slackness of 1.5%.

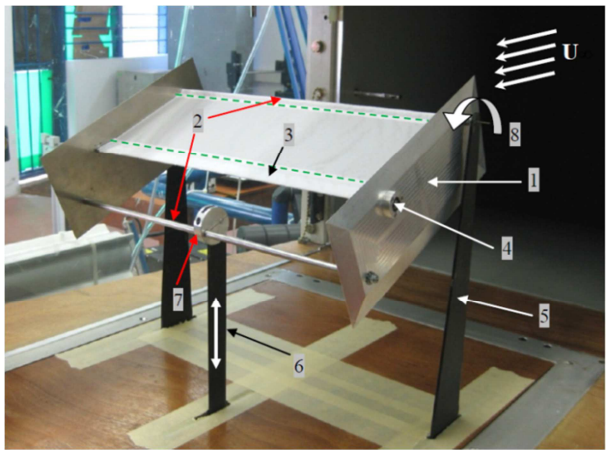

Figure 3 - Test rig with a sail as used in the experimental setup [18] .

The position and attitude of the plate of the trailing edge is taken from the measured data and used as input for the geometry of the numerical simulations. The geometry of the leading edge is constructed from the diameter of the mast and lines that are tangent to this mast corresponding to the cloth of the sleeve around the mast. In the numerical simulations this part of the geometry is fixed as well. The attitude of mast and trailing edge vary for each case and are therefore adjusted for each numerical simulation.

The initial shape of the cloth (red) is constructed from the arc of a circle with a length equal to the length of the undeformed cloth between the sleeves in the experiment. Please note that this length is not necessarily equal to the length of the sail shape in the experiment, since the experimental data shows the deformed sail shape. This becomes clear in Figure 4 from the difference in arc length between the red line and the blue line.

Figure 4 – Deformed experimental result (blue dots) and the geometry used for numerical simulations: The deformable part in the simulation is shown in red (dashed). The fixed leading and trailing edge are shown in black (continuous).

The flow conditions for the 2D case are tabulated in Table 4:

Table 4 – Flow conditions for 2D FSI simulations.

Air dynamic viscosity (Pa·s)	$1.85 \cdot 10^{-5}$
Air density (kg·m^{-3})	1.2
Air speed (m·s^{-1})	20
Reynolds number (-)	$1.78 \cdot 10^{5}$

2.5 3D GEOMETRY AND FLOW CONDITIONS

The geometry used for 3D numerical simulations has a span (height) of the sail of 10.5 m. The maximum chord is 4 m at the foot of the sail. The head of the sail is 0.2 m. the total surface area is 28.07 m^2. The angle of attack is constant with height and has a value of 5°. Commonly sails are designed with twist. However, since the CFD method does not account for a variation in wind speed and direction with height above the water surface, it was chosen to maintain a constant angle of attack by removing the twist in the sail. A mast is not incorporated in this geometry definition yet. This can be added to the geometry at a later stage. Flow conditions are tabulated below. The value for the Reynolds number is based on the maximum chord length.

Table 5 – Flow conditions for 3D FSI simulations.

Air dynamic viscosity (Pa·s)	$1.85 \cdot 10^{-5}$
Air density (kg·m^{-3})	1.2
Air speed (m·s^{-1})	8
Reynolds number (-)	$2.08 \cdot 10^{6}$

3 STRUCTURAL METHOD

Sails are made of thin cloth with anisotropic material properties. These cloths are exposed to a laterally distributed load. This causes large deflections, i.e. deflections that are as large as multiples of the thickness of the cloth. This renders the structural problem non-linear.

The code used for the structural analysis is the Nastran-based Femap v10.0 package. The sail is discretized using plate elements. These elements have resistance against bending. Four-noded quadrilateral (CQUAD4) elements are used to discretize the geometry.

From the mesh study it follows that for the 2D case a mesh with 100 elements along the chord of the sail is sufficient to obtain a mesh independent solution of the deformation. For the 3D case a mesh with 20x20 elements was used. This is a very coarse mesh. Literature recommends at least 15,000 elements in total [9]. Such a large mesh leads to time consuming interpolations of the pressure fields, therefore meshes of this size were not used for the actual FSI simulations in the present study. The mesh for the 3D sail should therefore be considered as crude and further development of the structural method is required.

A nonlinear static analysis is performed to solve for the deformation of the plate under uniform lateral load. 75 increments or load steps are adopted with a maximum of 25 sub-iterations per load step. For the 2D case the cloth has a thickness of 62 µm. An isotropic linear elastic material model was adopted. The stiffness of the cloth was varied between E = $73.5 \cdot 10^6$ N/m^2 and $147 \cdot 10^6$ N/m^2 and the Poisson ratio was set to ν = 0.3. This is representative for the nylon spinnaker cloth used in the experiments by Yam et al. For the 3D case the sail has an -modulus of $1.667 \cdot 10^9$ N/m^2 and a Poisson ratio of 0.3, representative for Dacron sail cloth. The thickness used is 5 mm, relatively thick compared to cloth used for sails. This was chosen in order to prevent large deformations that cannot be handled by the mesh deformation algorithm as currently implemented.

4 FSI COUPLING

Fluid structure interaction covers the coupled system of fluid and structural mechanics. The behaviour in the fluid domain can influence the behavior in the structural domain and vice versa. The structure can move or deform due to flow phenomena on its turn. The structure influences the flow behaviour in its turn. The flying shape of the sail is determined by FSI. The flow field and the structural deformation balance each other. This balance can be both steady and unsteady.

4.1 PRINCIPLE OF FSI COUPLING

A steady staggered weak FSI coupling is established. This means that the deformation field on one hand and the pressure field on the other hand are solved independently, by specialized solvers. The main advantage of this approach is that readily available and optimized numerical methods can be used. For this approach an exchange of information at the interface between the domains is required. Iterations are performed until convergence is reached.

4.2 SCHEME

A schematic representation of the FSI scheme is shown in Figure 5. This scheme consists of the following steps:

1. With the initial geometry and specification such as flow properties and structural properties two numerical simulations are set-up. A CFD computation is defined in FINE/Marine and a FEA computation in Femap. For both the application of the CFD method and the application of the FEM method a mesh is defined. All parts of the method that are identical for each iteration are defined in this step.
2. Using the initial mesh for the CFD method a CFD analysis is started for the initial geometry. This analysis leads to a pressure distribution on the surface of the sail. This part of the numerical procedure is written in Python.
3. The FEM method uses the pressure field from step 2 to define a load on the initial geometry and a numerical simulation is started. This leads to a deformation field. This part of the numerical procedure is written in VB.NET.
4. The deformation field is compared with the deformation field of the previous iteration. If the convergence criterion is met, convergence is achieved and the final (flying) shape of the sail is found. If convergence is not achieved the FSI cycle continues with step 5. For the first iteration no previous deformation field is available so the check on convergence is omitted.
5. The displacement field is only defined in terms of the coarse FEM grid. To define the deformed shape for the finer CFD grid an interpolation is required. This is performed using radial basis function interpolation This part of the numerical procedure is written in Matlab.
6. The FSI iteration number is increased by 1.
7. The geometry of the new iteration is written from the interpolated displacement field to a so called ITS-file. This is the geometry definition format for the input for the CFD method.
8. Using the definition of the deformed geometry step 2 is started again. The CFD method takes care of the mesh deformation. This step completes the cycle. This cycle is repeated until the convergence criterion is met.

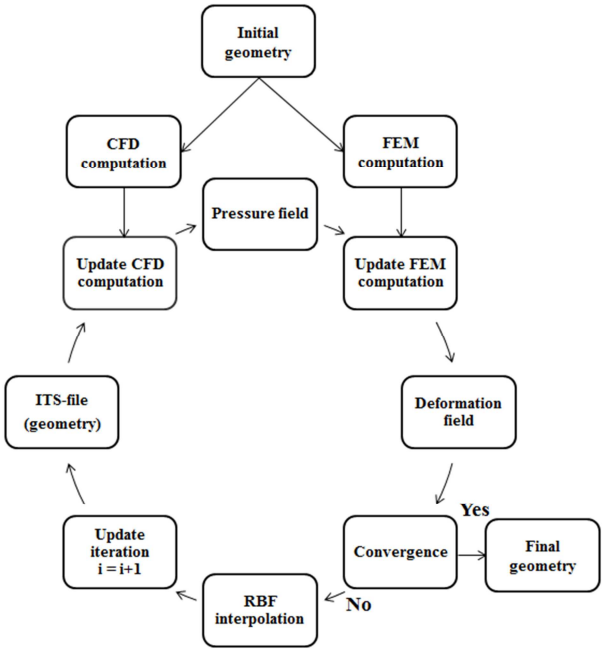

Figure 5 – Schematic representation of developed FSI method.

4.3 INTERPOLATION

The flow solver and the structural solver use different meshes. To be able to transport quantities (deformations/pressures) over the interface between the non-matching grids interpolation is required.

Radial Basis Function (RBF) interpolation is used for the interpolation of the deformation to the flow domain. RBFs are functions whose value depends on the distance from a sample point:

Sums of radial basis functions can approximate function values at random points:

RBFs have been used for example by Lombardi et al. [12] for the interface between the fluid and structural domain. According to Smith, Hodges and Cesnik [19], RBF interpolation with thin plate splines (TPS) is the most accurate and robust method to transfer information between non-conforming meshes. This is confirmed by De Boer, Van Zuijlen & Bijl [20], who favor RBF with TPS over other methods because of the accuracy and the simple algorithm of such an approach.

The second interpolation is the interpolation of the pressure data to the structure. A function with which to do this is already present in the used code Femap used for the structural problem. Interpolation is performed via a "Modified Inverse Distance Weighted Interpolation" [21]. Locations at which pressures are known, are provided to the method and interpolated to a data surface with the pressure data in the FEA domain.

5 RESULTS

The results of the first FSI calculations are presented in this chapter. An overview of the performed numerical simulations for the 2D test case is given and the simulation capabilities for 3D test cases are demonstrated.

5.1 2D RESULTS

Only a selection of experimental cases was steady enough to serve as test case for numerical simulations with the currently developed method. Numerical simulations have been performed for assessing the effect of three parameters:

- The slackness $s = \varepsilon/c = (l - c)/c$ was varied in accordance with the experiments.
- The angle of attack was varied in a certain range.
- The E-modulus of the cloth of the sail. Since the material properties of the cloth are not available, a sensitivity study has been performed to assess the effect of the stiffness of the cloth on the flying shape of the sail. The used values of the E-modulus are based on values used for similar purposes as found in literature [11] [22].

An overview of the runs with their specifications is tabulated below. For each run the depth of the sail for the initial (unloaded) and final (loaded) geometry is given. The last column shows the maximum error between the numerically determined flying shape and the experimentally determined flying shape as a percentage of the chord length.

Table 6 - Overview of numerical simulations of 2D sail. Re = $1.78 \cdot 10^5$.

	α (°)	s (-)	E-modulus (MPa)	Depth (initial)	Depth (final)	Max error
1a	4.5	1.5	294	2.04%	3.56%	1.85%
1b	4.5	1.5	147	2.04%	4.35%	1.05%
1c	4.5	1.5	73.5	2.04%	5.45%	0.46%
2	6.4	1.5	73.5	2.69%	5.76%	0.48%
3	8.4	1.5	73.5	2.67%	5.74%	0.45%
4	6.5	2.9	73.5	5.89%	7.81%	0.78%
5	6.6	4.4	73.5	8.55%	9.87%	0.54%

Cases 1a to 1c show the effect of the variation of the E-modulus of the cloth on the flying shape and on lift and drag. A clear dependence of the deformed shape on the stiffness of the sail is shown. From the three cases the flying shape with the lowest value of the E-modulus has the best correspondence with the experimentally observed flying shape. Therefore this stiffness was used for the remaining cases.

Case 1c to 3 show the effect of the variation of the angle of attack on the flying shape and lift and drag. The angle of attack is increased by approximately 2 degrees in each run. There is no substantial variation in the deviation between experimental and numerically determined flying shape. This shows the good predicting qualities of the FSI method within the range of angles of attack considered. For larger and smaller angles of attack unsteady effects were present in the experimental setup which cannot be accounted for accurately by the present numerical FSI method. The method can be extended to cover unsteady simulations if needed.

Cases 2, 4 and 5 show the influence of the variation in the slackness of the cloth on the flying shape and lift and drag. The increased slackness causes deformations to become larger. Generally this leads to a slightly lower accuracy in the numerical prediction of the flying shape but the results are still within acceptable accuracy (error less than 1%).

5.2 3D RESULTS

Numerical simulation for 3D FSI has been performed to investigate the capabilities of the present FSI method. The FEA mesh of the 3D sail is very crude and requires further improvement to be capable of predicting the flying shape of a 3D sail more accurately. Since experimental data is not available for this case, a validation could not be performed.

The deformation field of the sail is shown in Figure 6. In this figure the sail is given by coloured dots and the deformation field is represented by blue arrows. This is the deformed shape after 9 iterations. It can be observed that the leech of the sail stretches and bends away from the wind. This is the location where the largest deformation occurs. Along the luff or leading edge deformation to windward occurs indicating a too small angle of attack. The sail should be sheeted in more. The top and foot of the sail show large deformations. This can be due to tip vortices at each end of the foil/sail or due to the coarse FEM mesh.

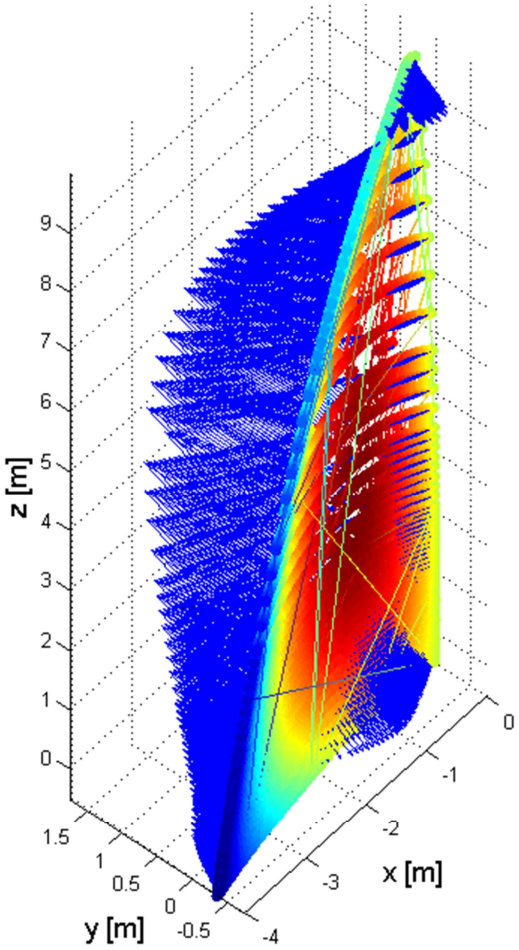

Figure 6 – Displacement vectors of deformed shape of 3D sail. Vectors are magnified for visibility.

When the deformed shape is examined more closely near the tack of the sail ripples are observed. These are visualized in Figure 7. The grey sail is the original un-deformed sail and the red sail is the deformed sail shape. These ripples are caused by the interpolation of the deformation data. This is an indication that more sample points (and thus a finer FEM mesh) are required for more accurate interpolation of the deformation.

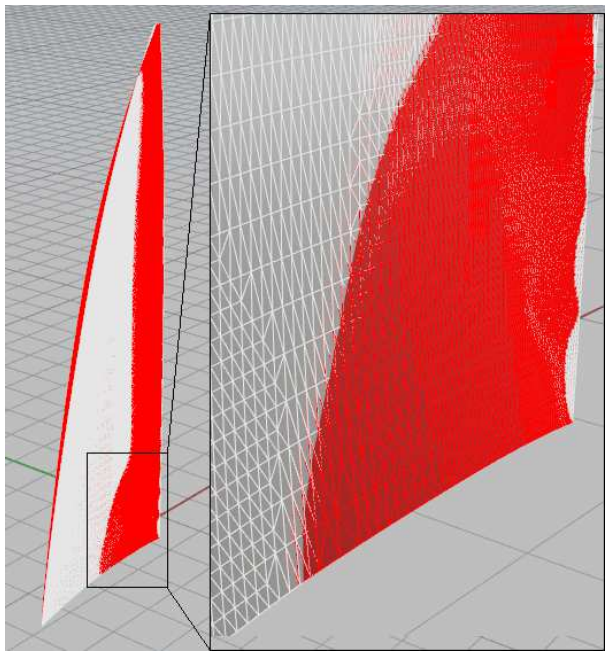

Figure 7 - Ripples at leading edge near tack of deformed shape of 3D.

6 CONCLUSIONS

The aim of this research was to develop a Fluid Structure Interaction method for yacht sails. This has resulted in a method that is capable of predicting flying shapes for sails for both 2D and 3D cases.

A steady segregated coupling is established to make optimal use of the available CFD and FEA packages.

The flow field is determined by solving the RANS equations using FINE/Marine CFD package employing the SST-Menter turbulence model. A mesh study was presented for the 2D case. Mesh deformation is used to deform the mesh according to the deformed shape of the sail. The pressure distributions obtained for deformed meshes are validated with pressure distributions obtained for un-deformed meshes.

Comparison of the results of the 2D case with experimental values shows good agreement in terms of deformation. It should be remarked that the application of a boundary layer method that includes a laminar-turbulent transition model could improve the prediction of the drag coefficient.

A coarse FEM mesh for computing the deformation of the sail under the aerodynamic load has been developed. The sail is discretized using four-noded quadrilateral elements. For the material properties linear isotropic homogenous material properties are chosen.

Interpolation of the deformation field across the non-conforming meshes of the fluid and structural domain is performed using Radial Basis Function interpolation. Errors in the interpolation can be reduced by using finer FEA meshes or increasing the number of sample points near the edges of the sail.

FSI analysis of 2D geometries has been performed and has been compared with available experimental data. Several runs have been performed to tune the unknown material properties of the sail cloth. For several angles of attack and slackness of the sail cloth good agreement has been found with experimental data. Differences between experimentally and numerically determined flying shapes amount to 0.8% of the chord length.

FSI analysis of a 3D geometry has also been performed, showing the capabilities of the FSI method to predict a flying shape for this specific geometry. The predicted deformation of the sail is in agreement with the expected flying shape, but experimentally obtained flying shapes are not available for validation. When assessing the flying shape it should be taken into account that a crude FEM mesh for the sail was used which should be improved to predict the flying shape more reliably.

ACKNOWLEDGEMENTS

The authors would like to thank Maor Yam for providing experimental data on their study to the deformation of 2D sails. The comparison of the results of the present method with experimental results would not have been possible without his experimental data.

The Numeca support team and Benoit Mallol are thanked gratefully for their very quick response on support issues and for providing a pre-release with essential capabilities for meshing sails. Their enthusiastic reactions to our results were encouraging.

REFERENCES

1. Fossati, F., 'Aero-Hydrodynamics and the Performance of Sailing Yachts'. *London : Adlard Coles Nautical*, 2009.
2. Schoop, H., 'Structural and Aerodynamic Theory for Sails'. *Eur. J. Mech. A/Solids 9(1)*, 1990.
3. Schoop, H. & Hänsel, M. 'Structural and Aerodynamic Calculation of Sails as Flexible Membranes', *Ship Technology, Vol. 44*, 1997.
4. Schoop, H., Bessert, N. & Taenzer, L., 'On the Elastic Membrane in Potential Flow', *Int. J. For Numerical Methods in Engineering, Vol 41*, 1998.
5. Fukasawa, T. & Katori, M., 'Numerical approach to Aeroleastic Responses of tree-dimensional flexible sails', *The 11th Chesapeake Sailing Yacht Symposium, Annapolis*, 1993
6. Schoop, H. & Bessert, N., 'Instationary Aeroelastic Computation of Yacht Sails', *Int. J. Numer. Meth. in Engineering, Vol 52*, 2001.
7. Renzsch, H., Muller, O. & Graf, K., 'FlexSail - A Fluid Structure Interaction Program for the Investigation of Spinnakers', *Proc. Intl. Conference on Innovations in High Performance Sailing Yachts, Lorient*, 2008.
8. Renzsch, H. en Graf, K., 'Fluid Structure Interaction Simulation of Spinnakers - getting closer to reality', *Proc. 2nd . Intl. Conference on Innovations in High Performance Sailing Yachts*, 2010.
9. Paton, J., Morvan, H.P. & Heppel, P., 'Fluid Structure Interaction of Yacht Sails', *Proc. Intl. Conference on Innovations in High Performance Sailing Yachts*, 2008.
10. Chapin, V.G., de Carlan, N. & Heppel, P., 'A Multidisciplinary Computational Framework for Sailing Yacht Rig Design & Optimization trough Viscous FSI', *The 20th Chesapeake Sailing Yacht Symposium, Annapolis*, 2011.
11. Trimarchi, D., Turnock, R., & Taunton D.J., 'The Use Of Shell Elements To Capture Sail Wrinkles, And Their Influence On Aerodynamic Loads', *Proc. 2nd . Intl. Conference on Innovations in High Performance Sailing Yachts, Lorient*, 2010.
12. Lombardi, M., Cremonesi, M., Giampieri, A., Parolini, N. & Quarteroni, A., 'A strongly coupled Fluid-Structure Interaction model for wind-sail simulation', *4th High Performance Yacht Design Conference, Auckland*, 2012.
13. Augier, B., Bot, P., Hauville, F., Durand, M., Dynamic Behaviour of a Flexible Yacht Sail Plan, *Ocean Engineering, 66:32–43*, 2013.
14. Numeca International, 'Theoretical Manual Fine/Marine v2.3.', 2011.
15. Collie, S.J., Gerritsen, M. & Jackson, P. 'A review of Turbulence Modelling for use in Sail flow Analysis', *School of Engineering Report No. 603. Department of Engineering Sciences, University of Auckland*, 2001.
16. Abbott, I.H. & Von Doenhoff, A.E. 'Theory of Wing Sections', *Mineola : Dover Publications, Inc.*, 1959.
17. Wilkinson, S. 'Static Pressure Distribution over 2D Mast and Sails Geometry', *Marine Technology, Vol. 26*, 1989.
18. Yam, M., Karlin, B.E. & Arieli, R., 'Estimation of Two-Dimensional Sail Shape from Single Camera Images.', *52nd Israel Anual Conference on Aerospace Sciences, Tel Aviv Haifa*, 2012.
19. Smith, M.J., Hodges, D. H. & Cesnik, C.E.S., 'An evaluation of computational algorithms to interface between CFD and CSD methodologies', *AIAA paper 96-1400*, 1996
20. de Boer, A., van Zuijlen, A.H. & Bijl, H., 'Review of coupling methods for non-matching meshes', *Computer methods in applied mechanics and engineering. 196*, 2007.
21. PLM, Siemens, 'Femap Commands version 10.0.1', 2008.
22. Trimarchi, D. & Rizzo, C.M., 'A FEM-Matlab code for Fluid-Structure interaction coupling with application to sail aerodynamics of yachts', *13th Congress of Intl. Maritime Assoc. of Mediterranean, Istanbul*, 2009.

AUTHORS BIOGRAPHY

Friso Bergsma M.Sc. is CFD specialist at Van Oossanen Naval Architects. He is responsible for (hydrodynamic) optimization and various R&D projects. His previous experience includes full scale testing of sails at the University of Auckland.

Niels Moerke M.Sc. B.Eng. is Director/Naval Architect at Van Oossanen Naval Architects. He is responsible for the CFD department and small craft design. His previous experience includes design and optimization of various award winning sailing yachts.

Sebastiaan Zaaijer M.Sc. is CFD specialist/Naval Architect at Van Oossanen Naval Architects. He is responsible for optimization and research projects. His research focuses on optimization methods for the shape of the hull and appendages of yachts.

Prof. dr. ir. Harry Hoeijmakers is chairman of the research group Engineering Fluid Dynamics at the University of Twente. Among his research areas are fluid dynamics, aerodynamics of wind turbines, flow control for various applications and multi-phase flows for industrial applications.